

**Antecedent North Pacific Jet Regimes Conducive to the Development of Cool Season  
Continental U.S. Tornado Outbreaks**

An honors thesis presented to the  
Department of Atmospheric and Environmental Sciences,  
University at Albany, State University of New York  
in partial fulfillment of the requirements  
for graduation with Honors in Atmospheric Science  
and  
graduation from The Honors College

Jessica P. Blair

Research Mentor: Andrew C. Winters, Ph.D.  
Research Advisor: Ross A. Lazear, M.S.

April 2019

## Abstract

The occurrence of tornado outbreaks are often associated with considerable societal and economic impacts. The U.S. averages nearly 1000 tornadoes per year that result in 1500 injuries and 80 fatalities, many of which are associated with outbreak days. Additionally, one outbreak alone can cause millions of dollars in property damage. The location of these outbreaks can vary temporally throughout the cool season (September–May) and can vary substantially in terms of their severity.

This study focuses on continental U.S. tornado outbreaks during the cool season and their relation to the state and evolution of the North Pacific jet (NPJ) stream 0–5 days prior to an outbreak. Tornado outbreaks are identified as days in which 6 or more (E)F2+ tornadoes were observed during a 24-hour (1200–1200 UTC) period using storm reports available from the Storm Prediction Center. This identification scheme identified a total of 189 outbreak days between 1979 and 2017. Following their identification, outbreak days are classified based on the geographic region impacted by the outbreak, the season, and the Destruction Potential Index ranking of the outbreak (developed by Thompson and Vescio 1998) in order to determine the state and evolution of the NPJ that is most conducive to each class of outbreak.

The state and evolution of the NPJ that is most conducive to each class of tornado outbreaks are investigated using an NPJ Phase Diagram, which is developed from the two leading empirical orthogonal functions (EOFs) of 250-hPa zonal wind anomalies over the North Pacific during the cool season. The first EOF corresponds to a zonal extension or retraction of the exit region of the climatological NPJ, while the second EOF corresponds to a poleward or equatorward shift of the exit region of the climatological NPJ. The projection of 250-hPa zonal wind anomalies at one or multiple times prior to an outbreak onto the NPJ Phase Diagram provides an objective characterization of the prevailing NPJ regime prior to an outbreak. The analysis demonstrates that each NPJ regime can strongly impact the character of the large-scale flow pattern over North America, and that the location and severity of tornado outbreaks can vary as a function of the antecedent NPJ regime.

## Acknowledgments

Many people have helped me through the research process and through writing my thesis. Thank you to my wonderful advisors for their support and encouragement throughout my research. Without their guidance this project would not have gotten to the level at which it is today. They helped me think creatively about my project and fostered new ways for me to investigate the data. They were also a huge help in applying for and choosing a graduate school. Thank you!

I'd like to thank my classmates who have been a big support system during the writing process. A special thank you to my classmate, Chelsea, for your help with coding and your reassurance throughout this entire process.

And finally, a huge thanks to my parents who have been my biggest support system through the last four years of my undergraduate career. Their love and encouragement to pursue my dreams has gotten me to where I am today. Without them none of this would be possible.

## List of Figures

Figure 1: NPJ Regimes and their Associated Flow Patterns.....	22
Figure 2: Outbreak Event Centroids during the Cool Season.....	23
Figure 3: EOF1 250-hPa Zonal Wind Anomalies.....	24
Figure 4: EOF2 250-hPa Zonal Wind Anomalies.....	25
Figure 5: Schematic of NPJ Phase Diagram and Classification of Sectors.....	26
Figure 6: Spatial Coverage of Tornadoes by Month.....	27
Figure 7: NPJ Phase Diagrams Categorized by Season.....	28
Figure 8: Schematic of Classification by Geographic Region.....	29
Figure 9: NPJ Phase Diagrams Categorized by Location.....	30 & 31
Figure 10: NPJ Phase Diagrams for Top 20 DPI Events.....	32
Figure 11: SPC Storm Reports for 10 November 2002.....	33
Figure 12: SPC Convective Outlook for 10 November 2002.....	34
Figure 13: 10-day NPJ Trajectory for the Veteran’s Day 2002 Case Study.....	35
Figure 14a: 250-hPa Jet at 1200 UTC 07 November 2002.....	36
Figure 14b: 250-hPa Jet at 1200 UTC 10 November 2002.....	36
Figure 15: 500-hPa Vorticity at 1200 UTC 10 November 2002.....	37
Figure 16a: 850-hPa Temperature at 1200 UTC 10 November 2002.....	38
Figure 16b: 850-hPa Precipitable Water at 1200 UTC 10 November 2002.....	38
Figure 17: Sounding launched from Nashville, TN at 1800 UTC 10 November 2002.....	39
Figure 18: 950-hPa Frontogenesis at 0000 UTC 11 November 2002.....	40

## Table of Contents

<b>Abstract</b> .....	ii
<b>Acknowledgments</b> .....	iii
<b>List of Figures</b> .....	iv
<b>Introduction</b> .....	1
<b>Methods</b> .....	4
<b>Results</b>	
a. Outbreaks Classified by Season .....	8
b. Outbreaks Classified by Location .....	11
c. Outbreaks Classified by DPI Ranking .....	12
<b>Veteran’s Day 2002 Outbreak Case Study</b> .....	13
<b>Conclusions</b> .....	17
<b>References</b> .....	20
<b>Figures</b> .....	22

## **I. Introduction**

The occurrence of tornadic events often carries significant societal and economic impacts. The continental U.S. averages 1,000 recorded tornadoes per year, resulting in 1,500 injuries and 80 fatalities annually (NOAA NSSL). One single tornado can cause millions of dollars in damage over the course of a few minutes. Entire businesses and homes are often destroyed in these outbreak events, displacing a multitude of families. The occurrence of such outbreaks varies both spatially and temporally throughout the cool season (September–May), and this fluctuates as a function of the changing synoptic patterns observed throughout the cool season. The phase of the North Pacific jet (NPJ) largely influences the upper-level flow downstream over the continental United States and can substantially affect the characteristics of these synoptic patterns (Griffin and Martin 2017; Winters et al. 2019a,b).

Tornadic outbreaks and their synoptic-scale influences have been analyzed in a variety of past papers. A study was conducted by Thompson and Roundy (2013) looking at the relationship between violent tornado outbreaks in the spring and the phase of the Madden-Julian Oscillation (MJO). This study looked at how the position of tropical convection affected circulation patterns over the mid-latitudes, and how these circulations set up synoptic patterns conducive to the formation of tornadic outbreaks. They found that certain synoptic patterns prior to a tornadic outbreak were quite common. These synoptic patterns included an upper-tropospheric trough axis located west of an outbreak, an upper-tropospheric jet co-located with an area of surface pressure falls, and the formation of a deep surface cyclone which would act to advect moisture from the Gulf of Mexico at low-levels. The synoptic patterns described above were observed for

both tornadic and non-tornadic environments; however, tornadic outbreaks were observed to occur in environments with a more amplified 500-hPa flow pattern, stronger helicity, and greater vertical wind shear. The importance of these synoptic and mesoscale features was also noted by Mercer et al. (2012). Thompson and Roundy (2013) found that tornadic outbreaks in the spring (MAM) were twice as common when the MJO was in phase two, implying that the MJO was convectively active over the Indian Ocean.

Cook et al. (2017) studied the impact of the El Niño-Southern Oscillation (ENSO) on winter and early spring tornadic outbreaks (JFMA). ENSO largely determines the mean latitudinal position of the subtropical jet over the continental U.S, which in turn can significantly influence the synoptic set-up for these tornadic events. During El Niño conditions, upper-level jets were found to be abnormally strong and displaced further south, while during La Niña conditions the upper-level jets were displaced further north. This meridional shift in the upper-level jet affects the location of surface cyclone formations, low-level jet formation, and the formation of low-level temperature and moisture gradients. Cook and Schaefer (2008) observed that winters with a neutral ENSO pattern had a tendency for more frequent and stronger tornadic outbreaks when compared to those during the warm phase of ENSO. During La Niña years an increase in poleward moisture advection by the low-level jet was observed further north, which would increase the occurrence of tornadoes further north and east compared to climatology. During El Niño conditions tornadoes were observed to occur less frequently and were located at more southern latitudes.

These previous studies suggest that the occurrence of tornadic outbreaks can be closely linked to the state and evolution of the NPJ. In this study, the relationship between continental U.S. tornado outbreaks during the cool season and the state and evolution of the NPJ 0–5 days

prior to such outbreaks are analyzed. The evolution and phase of the jet during the five days prior to the outbreak largely determines where the initial low-pressure system forms, the direction and strength of the upper-level flow, and the formation of low-level moisture and temperature gradients. Winters et al. (2019b) looked at the impact various phases of the NPJ have on the downstream flow over the continental United States (Fig. 1). They found that jet extensions of the jet exit region compared to the climatological mean resulted in an anomalous upper-level trough to form over the central North Pacific, as well as the formation of anomalous ridges over northwestern North America and the subtropical North Pacific. This jet regime results in the formation of a surface cyclone off the west coast, which drives southerly geostrophic flow along the west coast, and the formation of warm temperature anomalies at low-levels. Jet retractions result in the formation of an anomalous upper-level ridge in the high-latitude North Pacific, and anomalous troughs over the northwestern U.S. and the subtropical North Pacific. This results in a split NPJ, and the formation of a surface anticyclone over north-central Pacific. This flow pattern results in low-level cold anomalies along the west coast of North America, and warm anomalies over the central North Pacific and over the south-central U.S.

Poleward shifts of the jet exit region feature an anomalous upper-level trough over the high-latitude North Pacific and an anomalous ridge over the subtropical North Pacific, pushing the exit region of the jet poleward of  $40^{\circ}\text{N}$ . This results in the formation of a surface cyclone off the southern coast of Alaska, which promotes southerly geostrophic flow over the Northern U.S. This southerly flow results in warm temperature anomalies at the surface for much of that region and promotes upper-level ridging over eastern Canada. Equatorward shifts of the jet exit region result in the formation of an anomalous upper-level ridge over the high-latitude North Pacific and anomalous troughs over the subtropical North Pacific and eastern Canada. These height

anomalies result in an equatorward deflection of the exit region of the NPJ near Hawaii and weaken the NPJ over the North Pacific in comparison to the other regimes. This large-scale flow is conducive to the formation of a surface anticyclone near the Aleutian Islands and northerly geostrophic flow over North America, leading to cold temperature anomalies at the surface. Southerly geostrophic flow upstream of the surface anticyclone, results in warm temperature anomalies at the surface over the Bering Strait and Gulf of Mexico.

The influence of the NPJ's phase and its evolution on severe weather outbreaks can be seen by considering the severity and location of tornadic outbreaks. In particular, the location of these outbreaks can vary temporally throughout the cool season, and the severity and location of these outbreaks can vary as a function of the antecedent NPJ regime. Following the identification of outbreak days, events were categorized by season, geographic region, and severity. Using the NPJ Phase Diagram developed by Winters et al. (2019b), the evolution and phase of the NPJ prior to each class of outbreaks were identified and analyzed. A case study on the Veteran's Day tornadic outbreak of 2002 was also conducted to provide insight into how the NPJ's phase and evolution provided the synoptic-scale ingredients for the event to occur.

## **II. Methodology**

Outbreak days were classified as a 24-hour period where six or more (E)F2 or higher tornadoes occurred. This definition is similar to that used by Thompson and Roundy (2013) to identify Violent Tornado Days (VTD). In choosing this definition, events with high societal impacts are isolated. These impacts can include anything from extensive damage and personal injuries to fatalities. This definition also discounts weaker tornadoes such as waterspouts and gustnadoes. Consequently, the tornadic outbreaks observed are strictly a result of strong

synoptic-scale forcing. The 24-hour period was focused on a 1200 UTC through 1200 UTC time frame. This was done to ensure that outbreaks that occurred later during the afternoon and into the night would be classified as one single outbreak day. This time frame was also chosen to overlap with the same time frame used in the Storm Prediction Center's Daily Convective Outlooks. Outbreak days were only examined during the cool season as this is when the NPJ is strongest, and in turn will have the greatest impact on the location and severity of tornadic outbreaks downstream over the continental United States. This study also looks only at the outbreak days between the years 1979 and 2017. Since all of the data used to identify these outbreak days comes from the Storm Prediction Center's storm report database, it is important that the data used for the definition of a tornadic outbreak is consistent over this time period. From this definition, 189 outbreak days were identified.

In this study it is important to limit the influence of known secular trends in the tornado data. In the early 1970's there was a shift in the responsibility of reporting tornadoes from Federal and state climatologists to the National Weather Service (Brooks and Craven 2002). This resulted in a significant decrease in EF2 and higher tornadoes since the early 1970s (Verbout et al. 2006). In choosing the start of the analyzed period to be 1979, the methods in which severity classes were determined are consistent throughout the analyzed period. One inconsistency of the database during this time period is how the path width of a tornado was reported. Prior to 1995 the mean path width of tornado events was reported, however, starting in 1995 the database began reporting maximum path width. In Agee and Child (2014), the annual mean values of significant tornado path widths for the two periods were plotted. They found a discontinuity jump in their respective lower thresholds of path width of approximately 209 meters. In an attempt to equate these two populations of tornadoes, 209 meters were added to the mean path width of the events

prior to 1995 and are reclassified within the dataset as “maximum path width”. This methodology was applied to this study.

Outbreak days were then ranked using a Destructive Potential Index (DPI) to identify the events with the highest societal impacts. The DPI was developed by Thompson and Vescio (1998) and is defined as:

$$DPI = \sum_{i=1}^n a_i(F_i + 1)$$

where  $n$  is the number of tornadoes on any given outbreak day,  $a_i$  is the tornado damage area (this is equivalent to the path length multiplied by the path width), and  $F_i$  is the Fujita scale rating for each tornado. To find the DPI for each individual tornado one would simply solve  $a_i(F_i+1)$ , while the total DPI for the outbreak day would be the summation of each individual tornado’s DPI that occurred during one of the identified outbreak days. For each identified outbreak day, all tornadoes were accounted for in this summation including F0- and F1-rated tornadoes. The DPI was also used to create centroids for each outbreak day (Fig. 2). These centroids represent the weighted average of the starting locations of all the tornadoes on a given outbreak day. By using DPI as the weights, the location of the centroid for an outbreak day would be more heavily weighted towards the location of the higher impact tornadoes. Outbreak days were categorized and analyzed by season, geographic location, and DPI ranking. The latitude and longitude of the centroids for each event were used to categorize these events geographically. Once categorized, these events were analyzed using the NPJ Phase Diagram.

The NPJ Phase Diagram uses 250-hPa zonal wind anomalies from the 0.5°-resolution National Centers for Environmental Prediction Climate Forecast System Reanalysis (CFSR; Saha et al. 2010, 2014). These anomalies were recorded at 6-hour intervals during the cool

season 1979–2014. The 36-year mean was removed from the instantaneous 250-hPa zonal wind, as well as the annual and diurnal cycles, in order to calculate and identify these anomalies. A traditional EOF analysis was performed on the zonal wind anomalies within the domain of 10–80°N and 100°E–120°W. This domain was chosen to identify the two leading modes of variability for the NPJ. The two leading modes of variability obtained from the EOF analysis can be expressed as EOF1 and EOF2. A positive EOF1 (+EOF1) pattern is associated with a zonal extension of the jet-exit region when compared to the climatological mean, while a negative EOF1 (-EOF1) pattern is associated with a zonal retraction of the jet-exit region when compared to the climatological mean (Fig. 3). A positive EOF2 (+EOF2) corresponds to a poleward shift of the jet-exit region in comparison to the climatological mean, while a negative EOF2 (-EOF2) corresponds to an equatorward shift of the jet-exit region in comparison to the climatological mean (Fig. 4). The 250-hPa zonal wind anomalies at any given time can be projected onto EOF1 and EOF2 to calculate the instantaneous principal components (PCs), PC1 and PC2 that correspond to that time. The magnitude and sign of PC1 and PC2 are used to illustrate how strongly the instantaneous 250-hPa zonal wind anomalies project onto EOF1 and EOF2, respectively. The sign and magnitude of PC1 and PC2 can subsequently be plotted on the NPJ Phase Diagram. Positive values of PC1 correspond to a positive EOF1 and a jet extension of the jet-exit region in comparison to the climatological mean, while negative values correspond to a jet retraction. Positive values of PC2 correspond to a positive EOF2 and a poleward shift of the jet-exit region in comparison to the climatological mean, while a negative value corresponds to an equatorward shift. Anything which falls within 0.5 PC units of the origin of the NPJ Phase Diagram is considered neutral. A depiction of the North Pacific Jet Phase Diagram is provided in Fig. 5. For this study, PCs were analyzed 0–5, 0–10, and 3–7 days prior to an outbreak. The

mean of these PCs over each specified time interval was plotted for each of the outbreak days on the NPJ Phase Diagram. A single composite trajectory was also calculated by averaging the PCs over all events at 6-h intervals during the specified time window prior to outbreak initiation.

### **III. Results**

#### **a. Outbreaks Classified by Season**

Seasonally, these outbreaks were categorized into fall, winter, and spring outbreak events. Fall outbreak events were outbreak days which fell during the months of September, October, and November. Winter outbreak days were classified as those which fell within the months of December, January, and February. Spring outbreak days were classified as events which occurred during the months of March, April, and May. Upon examining the spatial coverage of tornadoes from month-to-month, a few interesting patterns were observed (Fig. 6). Fall tornadoes were mainly clustered along the Mississippi River valley. In September, there was a secondary cluster located over Virginia and southern Pennsylvania, while in October, there was a secondary cluster located over Indiana and Michigan. November had the most tornadoes during the fall season, and these tornadoes were not as spatially confined as the other two months during this period. Tornadoes during the winter season were very spatially confined to the southeast United States. This coverage stayed rather consistent during the three months within this season, with the majority of the tornadoes located within the state lines of Louisiana, Arkansas, Missouri, Mississippi, Alabama, Tennessee, Kentucky, and Georgia. The spring season was the least spatially confined in terms of tornadoes. This pattern was pretty consistent for all three months within this period, with tornadoes as far north as Minnesota and as far south as the Gulf Coast, ranging as far west as the Rockies and eastward towards the East coast. There were small

clusters of tornadoes within this large domain. In April, a cluster of tornadoes in Mississippi and Alabama were observed, while in May, this cluster was observed in the Southern Plains. These observed spatial and seasonal changes prompted the categorization of outbreaks by season and geographic location for further analysis.

In analyzing these categorized outbreaks, the 0–5-day period prior to an outbreak was used to analyze the state of the NPJ as it displayed the clearest signal compared to the other time periods considered. For the fall season, 33 outbreak days were identified, with majority of these events occurring in November. Fall outbreak days show a preference for poleward shifts and jet retractions of the jet-exit region 0–5 days prior to an outbreak when compared to the other NPJ regimes (Fig. 7a). There was also a large preference for the jet-exit region to take a neutral position in comparison to the other NPJ regimes. Of the 33 outbreak days identified, 30 percent showed a neutral preference, 24 percent showed a jet retraction, and 18 percent showed preference for a poleward shift. The mean starting position five days prior to the outbreak for the NPJ during the fall was located at (0.0894, -0.0105) within the NPJ Phase Diagram. This shows the mean starting position of the jet exhibits a slight jet extension, and a weak equatorward shift. When looking at the average evolution of the NPJ during the five-day period prior to these outbreaks, a strong movement towards a jet retraction was observed (Fig. 7b).

The winter season outbreaks had the fewest number of outbreak days with only 30 events. For the winter season, meridional shifts of the jet-exit region appear to be more prominent than zonal shifts (Fig. 7c). Winter outbreak days feature a strong preference for a poleward shift of the jet-exit region in comparison to the other NPJ regimes. The second most dominant NPJ regime was an equatorward shift of the jet-exit region. Of the 30 events that make up the winter season

category, 43 percent exhibited a preference for a poleward shift and 23 percent for an equatorward shift. Meanwhile, jet extensions and jet retractions made up only 7 and 17 percent of the winter events, respectively. The mean starting position of the NPJ five days prior to these outbreaks was located at  $(-0.2577, 0.498)$  within the NPJ Phase Diagram. This position indicates a jet whose exit region is both strongly retracted and shifted poleward in comparison to the climatological mean. The mean evolution of the NPJ prior to these outbreaks illustrates a poleward shift in the first few hours, which quickly transitions into a strong equatorward shift and jet extension by the time of event initiation (Fig. 7d).

The spring season had the largest number of outbreaks day with 126 events, with 60 of these events occurring in May. The spring season showed close to an equal split between all of the NPJ regimes prior to event initiation (Fig. 7e). However, a slight preference for a poleward shift and jet retraction was observed for this season. Of the 126 outbreak days, jet retractions made up 24 percent of the events and poleward shifts made up 22 percent of the events. The mean position of the NPJ five days prior to an outbreak was located at  $(-0.0389, 0.0244)$  within the NPJ Phase Diagram. This indicates the position of the NPJ at the start of the five-day evolution prior to an outbreak is both slightly retracted and shifted poleward. During the five-day period prior to event initiation, the jet evolves towards a very weak jet retraction and poleward shift (Fig. 7f). The inconclusive results from this season can be explained by the fact that the majority of the events for this season are during May. May is reaching the point in the year where the strength of the NPJ is heading towards its annual minimum. Consequently, out of all the months in the dataset, May and September are expected to have the weakest signals for the NPJ. This implies that outbreaks during these months would not be as synoptically driven as those during the winter months.

## **b. Outbreaks Classified by Location**

Spatially, outbreak events were broken up into four regions; the Northern Plains, Southern Plains, Northeast, and Southeast (Fig. 8). Outbreaks were placed in each of the four categories based on whether their centroids fell north or south of  $37^{\circ}\text{N}$ , and whether they fell east or west of  $90^{\circ}\text{W}$ . The observed relationship between the antecedent NPJ regime and outbreak location appeared to show the strongest correlation, especially with respect to the composite trajectories of the NPJ prior to these events. Northern Plains events made up 38 of the 189 outbreak events analyzed throughout this thesis. These events showed a preference for jet retractions, as well as for equatorward and poleward shifts during the five-day period prior to an outbreak (Fig. 9a). Of the 38 events that fall within this geographic category, 26 percent showed a preference for jet retractions, 23 percent for equatorward shifts, and 21 percent for poleward shifts. The mean position of the NPJ within the NPJ Phase Diagram five days prior to Northern Plains events shows a jet retraction and poleward shift, with the composite trajectory showing a strong evolution towards an equatorward shift over the five-day period prior to event initiation (Fig. 9b).

Southern Plains events made up close to half of the total outbreak days with 70 events falling within this geographic region. These events showed a preference for the NPJ to exhibit a poleward shift and a retraction of the jet-exit region during the 5-day period prior to an outbreak, with these two NPJ regimes making up 25 and 21 percent of the Southern Plains outbreak events, respectively (Fig. 9c). A large portion of the Southern Plains events also fell within a neutral NPJ regime, with 24 percent of these events falling within a 0.5 PC radius of the origin of the NPJ Phase Diagram. These events had a mean location within the NPJ Phase Diagram showing a

weak poleward shift and jet extension 5 days prior to event initiation. The composite trajectories prior to these events showed a strong evolution towards a jet retraction during the five-day period before an event (Fig. 9d).

Northeast outbreaks had the fewest events compared to the other three geographic regions with only 27 events. Northeast outbreak events showed a strong preference towards a jet retraction during the five-day period prior to event initiation (Fig. 9e). In particular, jet retractions made up 33 percent of the outbreaks in this geographic region. The average starting position of the NPJ within the NPJ Phase Diagram five days prior to an outbreak indicates both a strong jet retraction and equatorward shift of the jet-exit region. The composite trajectory for Northeast outbreaks shows an initial shift of the jet-exit region equatorward and shows an extension of the jet-exit region during the last few days of the evolution period (Fig. 9f).

Southeast outbreak days consist of 54 events. This geographic region showed the strongest preference for a particular NPJ regime during the five-day period prior to an outbreak. Poleward shifts of the jet-exit region were largely favored for this region, with 35 percent of the events exhibiting this NPJ regime (Fig. 9g). This NPJ regime was observed twice as often as any of the other regimes. The average location of the NPJ five days prior to an outbreak shows a strong poleward shift and weak jet extension. Over the 5-day prior to event initiation, the composite trajectory illustrates that the NPJ shifts poleward initially, and eventually retracts westward later on during the evolution (Fig 9h).

### **c. Outbreaks Classified by DPI Ranking**

The relationship between the antecedent NPJ regime and outbreak severity was also analyzed (Fig. 10a). The top twenty most destructive outbreaks were identified based on their DPI ranking. These events showed a preference towards poleward shifts and jet extensions during the five-day period prior to event initiation. Of the 20 events analyzed for this category, 35 percent of these events showed a poleward shift, and 30 percent exhibited a jet extension. The other three regimes equally make up the remaining 35 percent of the events. The average position of the NPJ 5 days prior to these outbreaks shows a jet extension and strong poleward shift of the jet-exit region. The trajectory of the jet during the five-day period prior to event initiation illustrates an initial shift towards a jet extension, which quickly evolves towards a strong jet retraction and equatorward shift (Fig. 10b). On the NPJ Phase Diagram, one event stands out among the rest, representing a strong jet extension (Fig. 10a). This event is the 2002 Veteran's Day Outbreak. A case study was conducted on this event to further analyze the role that the antecedent NPJ regime plays during such an outbreak.

#### **IV. Veteran's Day 2002 Outbreak Case Study**

The Veteran's Day Outbreak occurred on 10 November 2002. Out of the 189 outbreak events identified using our chosen definition of an outbreak, this event ranked as the 18<sup>th</sup> most destructive. This outbreak had 93 reported tornadoes, 190 large hail reports, and 332 wind damage reports. Tornadoes were reported across 11 states stretching from the Gulf Coast northward to the Great Lakes (Fig. 11). With its high DPI ranking, large societal impacts would be expected from this event. Over 200 injuries and 36 fatalities were reported as a result of this outbreak. Several hundred homes and businesses were completely destroyed, with property losses conservatively estimated to be several hundreds of millions of dollars across the region

(Midwestern Regional Climate Center 2002). The Storm Prediction Center issued a convective outlook at 0600 UTC on 10 November for the 1200 UTC–1200 UTC period beginning on 10 November, which placed a high risk for severe thunderstorms over northeast Mississippi, Tennessee, northwest Alabama, and a majority of Kentucky (Fig. 12). There was a moderate risk for the lower Ohio River valley, central portions of Mississippi and Alabama, northwest Georgia, eastern Kentucky and Tennessee, and far western Virginia and North Carolina. A slight risk was placed for the remaining regions extending from the Gulf Coast to the Great Lakes. Strong thunderstorms began to erupt shortly after 1200 UTC on the morning of 10 November 2002.

The 250-hPa jet and its antecedent phase over the North Pacific played a large role in determining the severity and location of this event. During the ten days leading up to the event, the mean 250-hPa jet exhibited a strong jet extension on the NPJ Phase Diagram compared to the climatological mean (Fig. 13). This aligns with the jet regime preferences for both the fall season and the most destructive outbreaks. This event projected strongly onto a jet extension, but very weakly onto one of the meridional shift NPJ regimes. Over the ten-day period prior to event initiation the jet remained quite zonal. Its ten-day trajectory showed the jet starting off rather zonal with a slight extension of the jet-exit region eastward (Fig. 13). Over the first five days of the evolution the jet-exit region began to shift slightly poleward and extended further east. Four days prior to the outbreak, the jet-exit region began to shift equatorward slightly but remained strongly extended. In the last two days leading up to the outbreak, the jet-exit region retracted westward with its ending location within the NPJ Phase Diagram similar to that of its starting position ten days earlier. This trajectory was very similar to that of the composite trajectory for the top 20 most destructive outbreaks, as well. The evolution of the jet prior to the outbreak largely determines where the initial low-pressure system forms at the surface, the direction and

strength of the upper level flow, the formation of surface temperature gradients, and how moisture will be advected at lower levels in the atmosphere. These factors all govern both the severity and location of the outbreak.

On 7 November, three days prior to the outbreak, a low-pressure system began to form over western Alberta, Canada. At this time the poleward exit region of the NPJ was located off the coast of Oregon, and was coupled with the equatorward entrance region of a secondary jet located over Northwestern Canada (Fig. 14a). This coupling acted to enhance the divergence of the ageostrophic wind in this region resulting in lower pressure at the surface. At this time, the jet was at its most zonal extension and the jet-exit region had begun to shift slightly equatorward (Fig. 13). This evolution of the NPJ helped to position the poleward exit region of the 250-hPa jet slightly south so that it would couple favorably with the equatorward entrance region of the Canadian jet. As the jet crossed the West Coast, the wind speeds in the jet core were close to 200 knots, which is anomalously strong for this time of year. The jet remained quite zonal over the next 24 hours, with the surface low remaining under the poleward jet-exit region, steering the surface low eastward along the Canadian/U.S. border.

On 8 November, a lee trough began to form downstream of the Rockies and a secondary low-pressure system began to form over Kansas by 0000 UTC 9 November. By the 1200 UTC 9 November, these two low-pressure systems merged. As the jet-exit region began to shift further equatorward by 10 November, a deep longwave upper-level trough began to form over the central U.S (Fig. 14b). The location of a trough to the west of an outbreak was noted as a key component for tornadic outbreaks in Thompson and Roundy (2013). This slow-moving and deep upper-level trough helped to facilitate moisture advection at the low-levels farther poleward.

During the outbreak, the region stretching from the Great Lakes to the Gulf Coast was located under the inflection point between the 250-hPa trough and a downstream ridge. The ageostrophic winds are known to diverge aloft at this inflection point and promote upward vertical motion. Jet coupling was also observed at this time over Michigan, Ohio, and Indiana, helping to strengthen the surface cyclone which was located over the Great Lakes at this time. This, too, was a key ingredient for an outbreak as identified by Thompson and Roundy (2013). Between the jet coupling and inflection point within the upper-level flow, upper-level divergence was maximized over this region.

In the mid-levels of the atmosphere, there were some contributions made to the upward vertical motion by cyclonic vorticity advection at 500-hPa. Cyclonic vorticity maxima were quite far removed from the surface low as it evolved, and vorticity advection did very little to deepen the surface low as it moved across the U.S during the three days leading up to the outbreak. However, cyclonic vorticity advection did play a larger role in the hours leading up to the outbreak. A concentrated area of cyclonic vorticity was located over the Northern Plains, with ribbons of cyclonic vorticity located over the Southern Plains at 1200 UTC 10 November (Fig. 15). The concentrated area of vorticity arose primarily from curvature, while the ribbons of vorticity were associated with speed shear. At this time, the winds at 500-hPa were predominantly westerly, resulting in cyclonic vorticity advection and promoting upward vertical motion over the outbreak region. These westerly winds also advected dry continental air at mid-levels toward the outbreak region.

At lower-levels, strong temperature and moisture boundaries began to form around 0000 UTC 10 November. As the jet exit region of the NPJ began to shift equatorward on 10 November,

facilitating the formation a deep trough aloft over North America, winds at lower levels became southerly. These southerly winds can be observed at 850-hPa advecting warm, moist air from the Gulf of Mexico as far north as the Canadian border (Figs. 16a,b). These anomalous 850-hPa winds are characteristic of a low-level jet, which was found to correlate with tornadic activity over the lower Mississippi, Tennessee, and Ohio River basins (Muñoz and Enfield 2009). With the warm, moist air close to the surface and the cooler dry air aloft, an elevated mixed layer was able to form, resulting in high instability over much of the region. This elevated mixed layer can be seen in the 1800 UTC 10 November sounding from Nashville, Tennessee (Fig. 17). The western extent of these temperature and moisture boundaries was quite sharp. This indicated an approaching surface cold front, with warm, moist southerly winds ahead of the front and cool, dry westerly winds behind the front. As the southerly winds ahead of the front increased, the temperature and moisture gradients began to intensify. This resulted in frontogenesis and for substantial upward vertical motions to develop within the lower levels of the atmosphere (Fig. 18). This low-level forcing for upward vertical motion would serve as the trigger to break through the capped environment. Vertical wind shear was also quite strong both due to speed and curvature shear. At 1200 UTC 10 November, winds over southern Illinois winds were southwesterly at about 40 knots, where winds aloft were 150 knots. This strong vertical shear is also known to be quite conducive to the formation of severe weather.

## **V. Conclusions**

The NPJ and its regime have been shown to influence the downstream large-scale flow pattern over the United States. The influence of the NPJ regime and its evolution can largely be seen by considering the severity and location of tornadic outbreaks. The strongest correlation

between the NPJ's antecedent regime and the occurrence of tornadic outbreaks was seen when events were analyzed by geographic location. Northern Plains events showed a preference for a jet retraction and equatorward shift, while the evolution of the NPJ prior to these events indicated a strong movement towards a poleward shift during the five-day period leading up to an outbreak. The presence of a jet retraction prior to an outbreak is conducive for a trough to form over the western United States, setting up low-level warm temperature and moisture advection over the Plains. Southern Plains outbreaks showed a preference for poleward shifts and jet retractions, with the composite trajectory showing an evolution of the NPJ towards a stronger retraction over the five-day period prior to outbreak initiation. Northeast outbreaks showed a strong preference towards a jet retraction, with the composite trajectory showing the NPJ shifting equatorward initially and eventually towards a jet extension. This evolution sets up a trough over the central U.S. and resultant low-level warm temperature and moisture advection over the Northeast. Southeast events had a strong preference for a poleward shift, and the composite trajectory showed a weak shift poleward and an evolution towards a jet retraction prior to outbreak initiation.

When analyzed seasonally, the winter months showed the strongest signal in the context of the NPJ Phase Diagram with a preference towards a poleward shifted NPJ, and a composite trajectory showing an evolution towards an equatorward shift and jet extension prior to event initiation. The most destructive outbreaks showed a rather strong signal as well. The preferred phase prior to these events was a poleward shift and jet extension, with the composite trajectory illustrating an evolution towards an equatorward shift and jet retraction by the time of outbreak initiation. As seen in the Veterans Day case study, the phase and evolution of the jet largely determined the location of surface cyclones, the direction and strength of the upper and low-level

flow, and the formation of low-level temperature and moisture gradients. These elements have been shown by previous studies as key synoptic-scale ingredients during the formation of such tornadic outbreaks.

Analyzing these synoptic patterns as a function of the prevailing NPJ regime would be the next step in this research project. This can be accomplished through performing a composite analysis of events that are preceded by the same antecedent NPJ regime. This would provide a way to examine whether the dynamical processes that lead to tornadic outbreaks differ as a function of the antecedent NPJ regime. These could be analyzed by season, geographic location, and outbreak severity to obtain a better understanding of how these synoptic patterns also vary based on these categories.

## References

- Agee, E. and S. Childs, 2014: Adjustments in tornado counts, F-scale intensity, and path width for assessing significant tornado destruction. *J. Appl. Meteor. Climatol.*, **53**, 1494–1505.
- Brooks, H.E., and J.P. Craven, 2002: A database of proximity soundings for significant severe thunderstorms: 1957-1993. Preprints, 21<sup>st</sup> Conf. on Severe Local Storms, San Antonio, Tx. *Amer. Meteor. Soc.*, 16.2.
- Cook, A.R. and J.T. Schaefer, 2008: The relation of El Niño–Southern Oscillation (ENSO) to winter tornado outbreaks. *Mon. Wea. Rev.*, **136**, 3121–3137.
- Cook, A.R., L.M. Leslie, D.B. Parsons, and J.T. Schaefer, 2017: The impact of El Niño Southern Oscillation (ENSO) on winter and early spring U.S. tornado outbreaks. *J. Appl. Meteor. Climatol.*, **56**, 2455-2478.
- Griffin, K. S., and J. E. Martin, 2017: Synoptic features associated with temporally coherent modes of variability of the North Pacific jet stream. *J. Climate*, **30**, 39–54
- Mercer, A.E., C.M. Shafer, C.A. Doswell, L.M. Leslie, and M.B. Richman, 2012: Synoptic composites of tornadic and nontornadic outbreaks. *Mon. Wea. Rev.*, **140**, 2590–2608.
- Midwestern Regional Climate Center, 2002: Severe weather outbreak - November 10, 2002.
- Muñoz, E., and D. Enfield, 2009: The boreal spring variability of the Intra-Americas low-level jet and its relation with precipitation and tornadoes in the eastern United States. *Climate Dyn.*, **36**, 247–259.
- NOAA National Severe Storms Laboratory. Severe weather 101: tornadoes.
- Saha, S., and Coauthors, 2010: The NCEP Climate Forecast System Reanalysis. *Bull. Amer. Meteor. Soc.*, **91**, 1015–1058.
- Saha, S., and Coauthors, 2014: The NCEP Climate Forecast System version 2. *J. Climate*, **27**,

2185–2208 .

Thompson, R. L., and M. D. Vescio, 1998: The destruction potential index—A method for comparing tornado days. Preprints, 19th Conf. on Severe Local Storms, Minneapolis, MN, *Amer. Meteor. Soc.*, 280–282.

Thompson, D.B. and P.E. Roundy, 2013: The relationship between the Madden–Julian Oscillation and U.S. violent tornado outbreaks in the Spring. *Mon. Wea. Rev.*, **141**, 2087–2095.

University of Wyoming. Atmospheric Soundings

Verbout, S. M., H. E. Brooks, L. M. Leslie, and D. M. Schultz, 2006: Evolution of the U.S. tornado database: 1954–2003. *Wea. Forecasting*, **21**, 86–93.

Winters, A. C., L. F. Bosart, and D. Keyser, 2019a: Antecedent North Pacific jet regimes conducive to the development of continental U.S. extreme temperature events during the cool season. *Wea. Forecasting*, **34**, 393–414

Winters, A.C., D. Keyser, and L.F. Bosart, 2019b: The development of the North Pacific Jet Phase Diagram as an objective tool to monitor the state and forecast skill of the upper-tropospheric flow pattern. *Wea. Forecasting*, **34**, 199–219.

## Figures

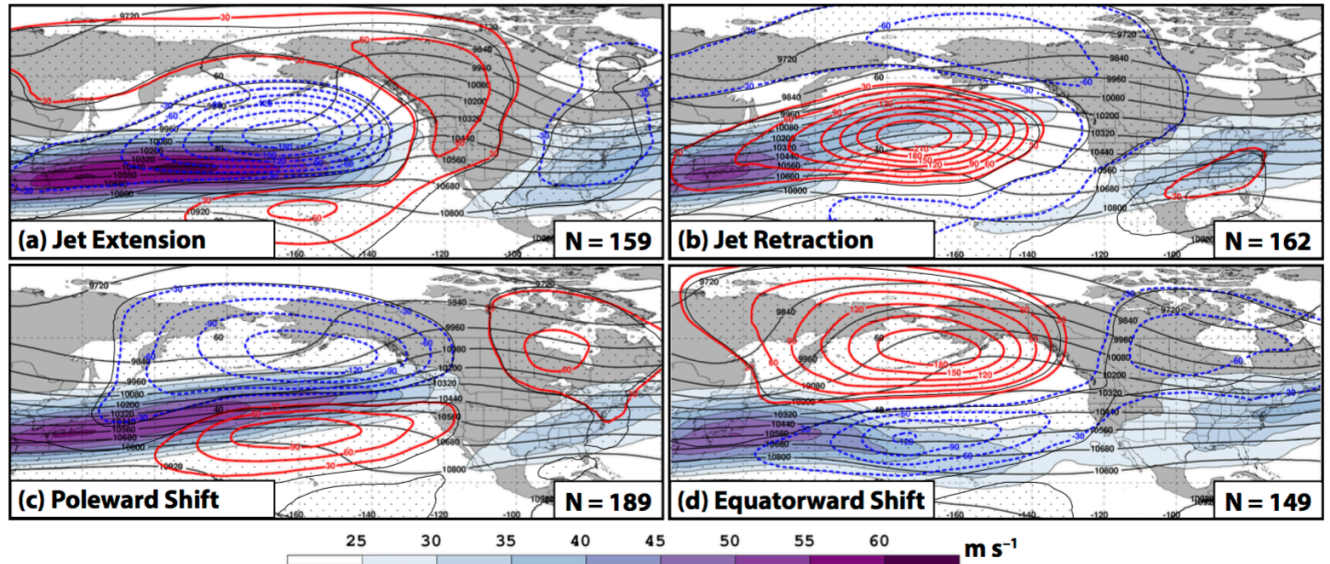


FIG. 1: Composite mean 250-hPa wind speed in  $\text{m s}^{-1}$  is shaded in the fill pattern, 250-hPa geopotential height is contoured in black every 120 m, and 250-hPa geopotential height anomalies are contoured in solid red and dashed blue every 30 m for positive and negative values, respectively, 4 days following the initialization of a (a) jet extension, (b) jet retraction, (c) poleward shift, and (d) equatorward shift regime. Stippled areas represent locations where the 250-hPa geopotential height anomalies are statistically different from climatology at the 99% confidence interval (Caption from Winters et al. 2019b).

## All Centroids 1979-2017

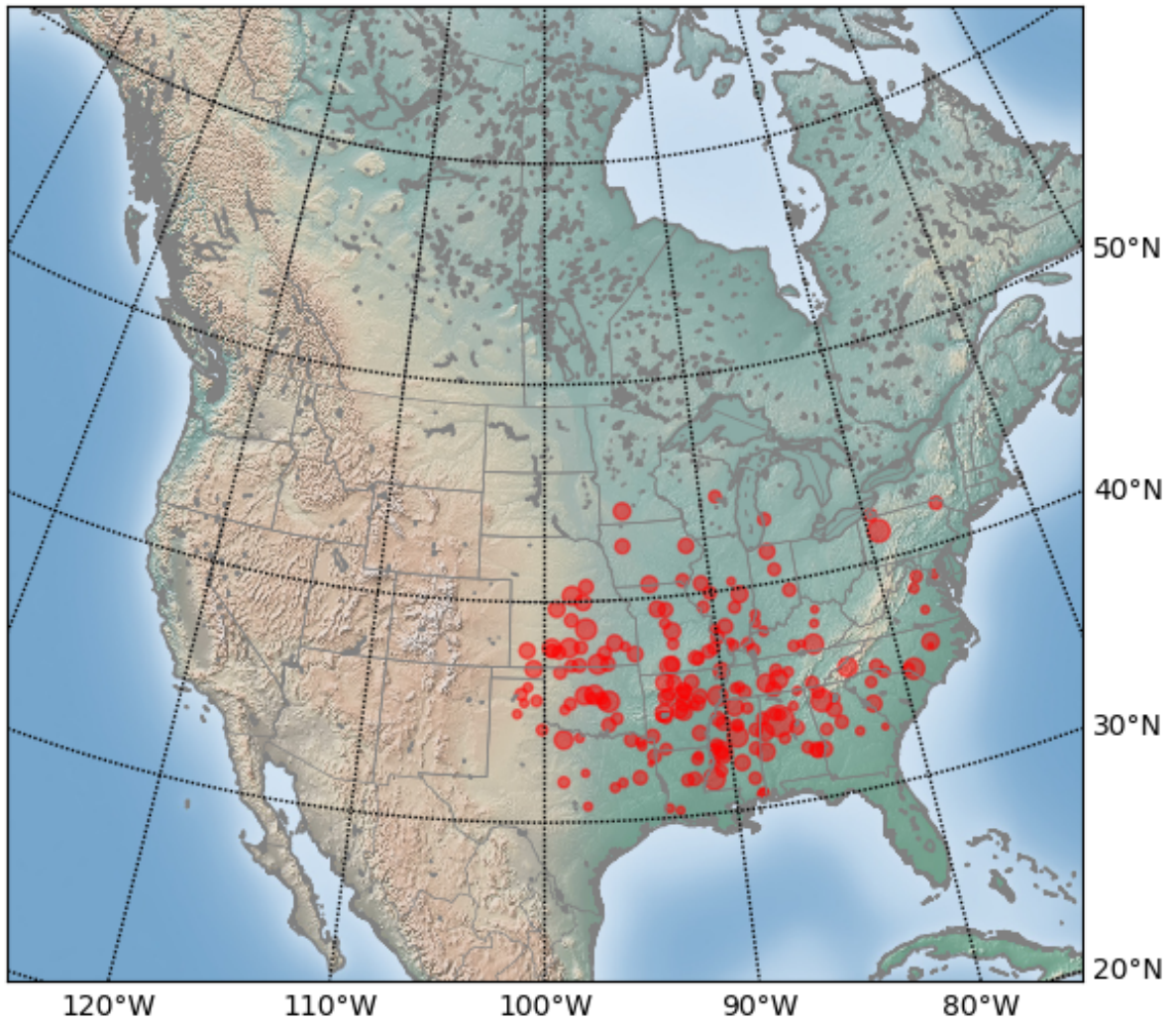


FIG. 2: Outbreak event centroids during the cool season, 1979–2017, with the size of each centroid scaled by its respective DPI ranking.

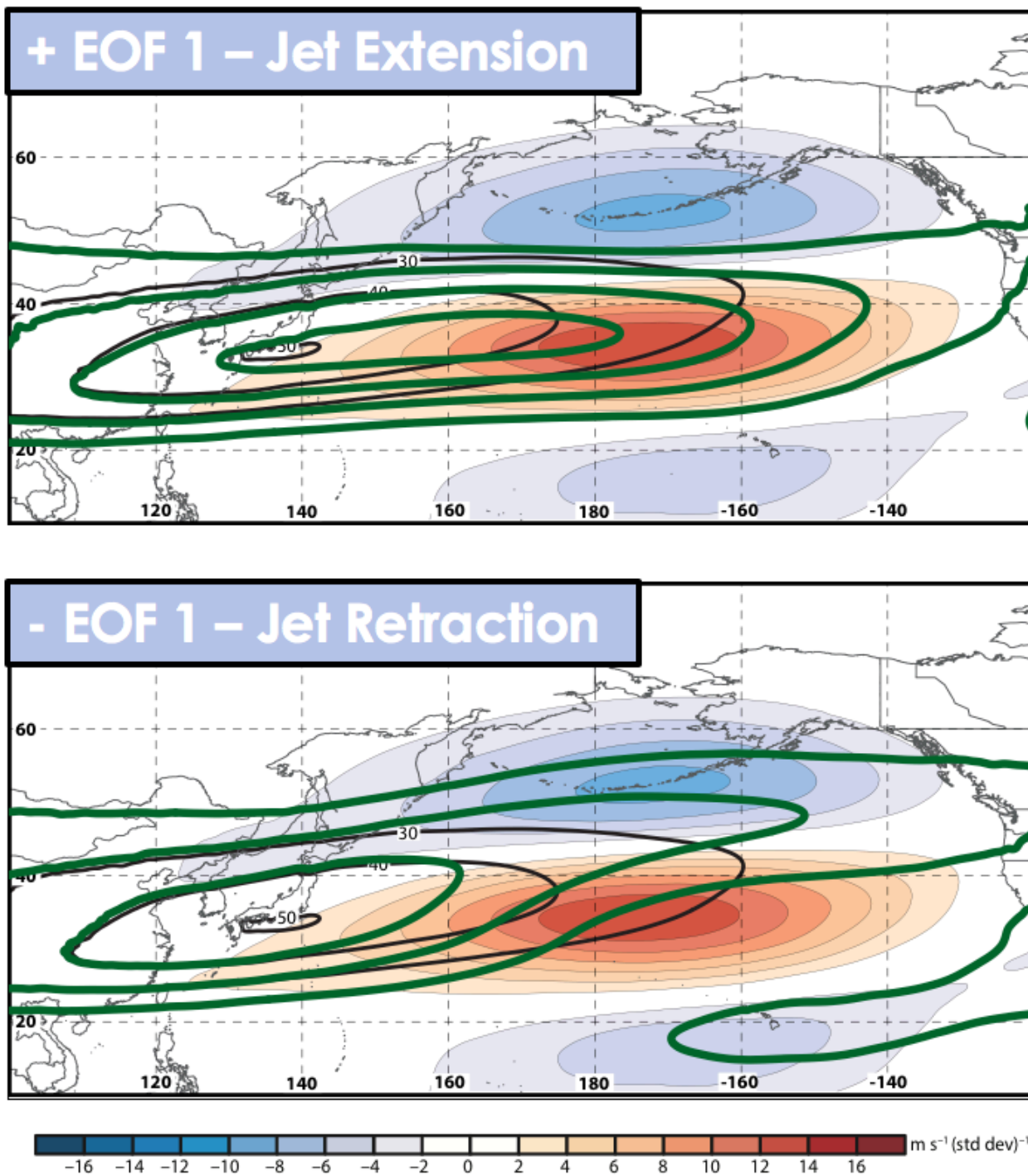


FIG. 3: September–May 250-hPa mean zonal wind contoured in black every 10 m s<sup>-1</sup> above 30 m s<sup>-1</sup> and the regression of PC1 onto 250-hPa zonal wind anomaly data (i.e., EOF1) is shaded following the legend in m s<sup>-1</sup>. Hypothetical zonal wind anomalies are contoured in green (Figure and caption adapted from Winters et al. 2019b).

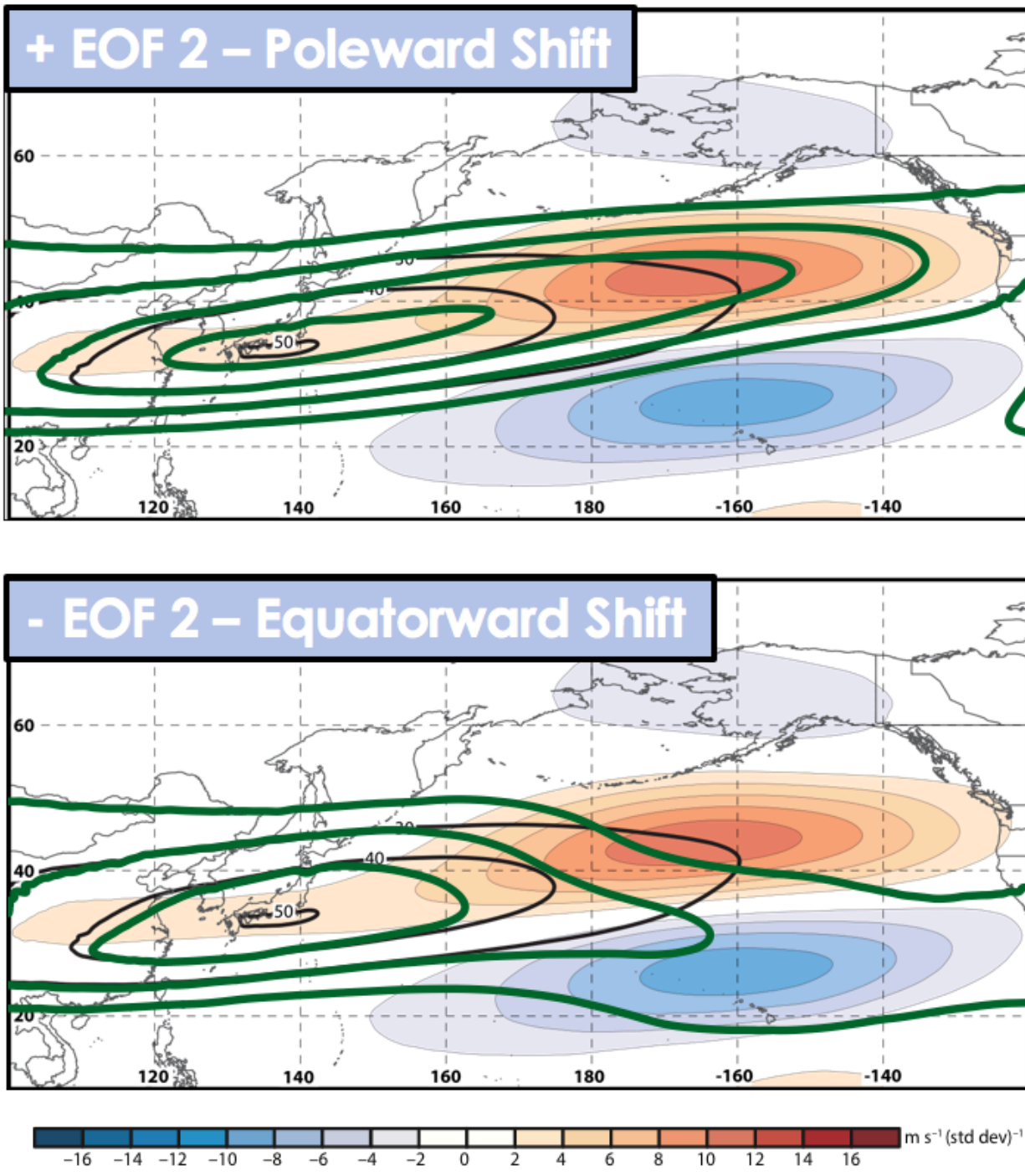


FIG. 4: September–May 250-hPa mean zonal wind contoured in black every  $10 \text{ m s}^{-1}$  above  $30 \text{ m s}^{-1}$  and the regression of PC2 onto 250-hPa zonal wind anomaly data (i.e., EOF2) is shaded following the legend in  $\text{m s}^{-1}$ . Hypothetical zonal wind anomalies are contoured in green (Figure and caption adapted from Winters et al. 2019b).

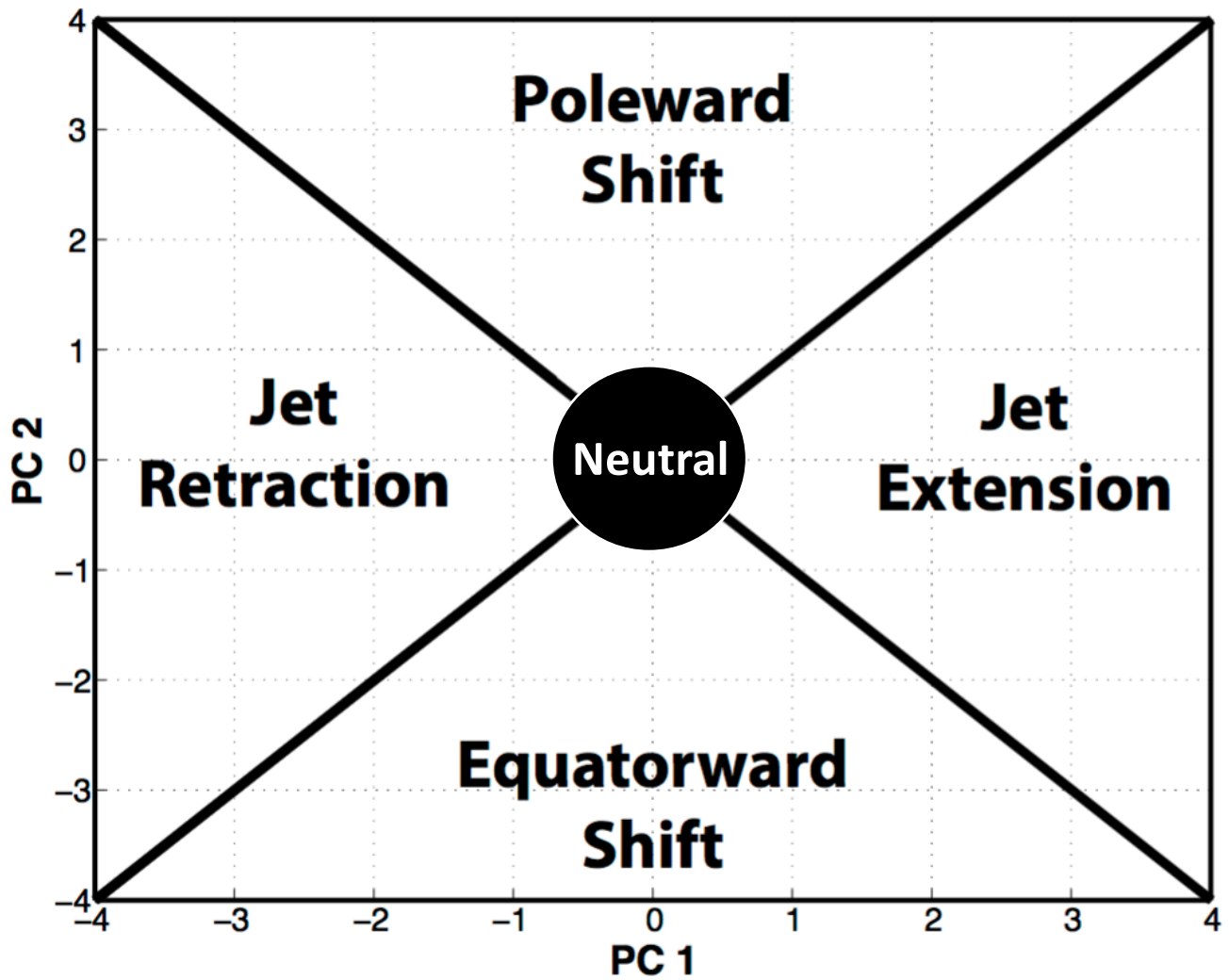


FIG 5. Schematic illustrating the classification scheme for the identified severe weather outbreaks.

September Tornadoes 1979-2017    October Tornadoes 1979-2017    November Tornadoes 1979-2017



December Tornadoes 1979-2017    January Tornadoes 1979-2017    February Tornadoes 1979-2017



March Tornadoes 1979-2017

April Tornadoes 1979-2017

May Tornadoes 1979-2017

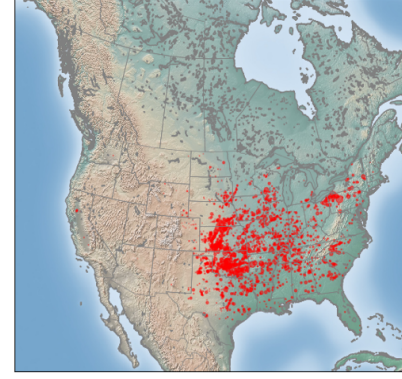
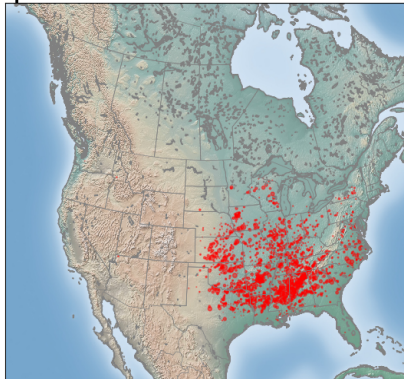
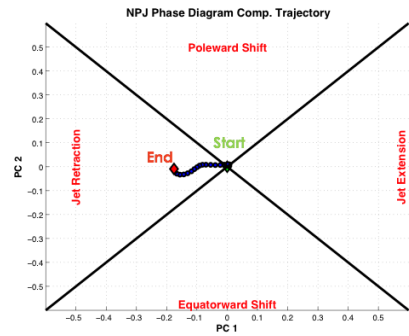
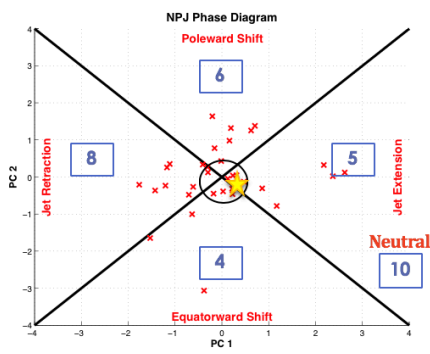
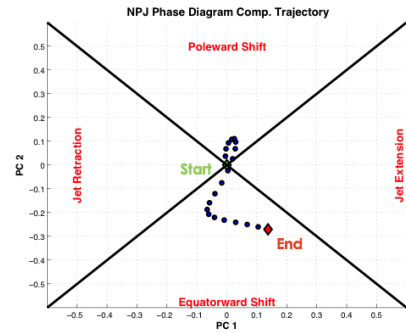
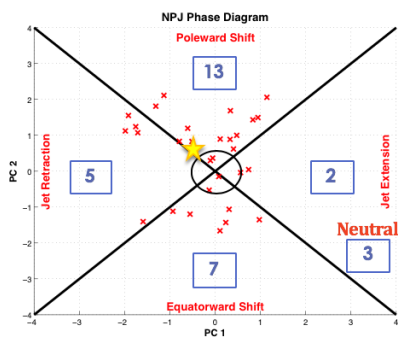


FIG 6. The spatial coverage of tornadoes for each month during the cool season. Individual tornadoes are denoted by red markers, with the size of each marker scaled by its respective DPI ranking.

a & b: SON season outbreaks (N=33)



c & d: DJF season outbreaks (N=30)



e & f: MAM season outbreaks (N=126)

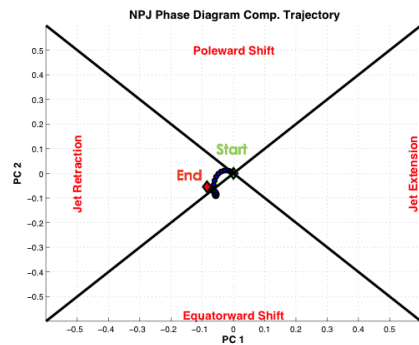
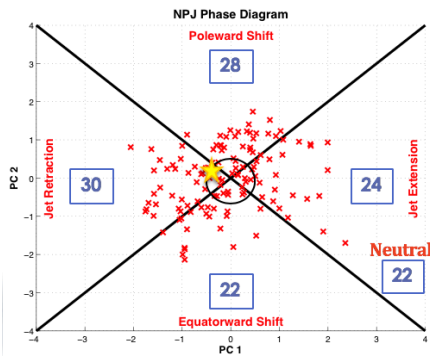


FIG 7. (a, c, & e) NPJ Phase Diagrams where each 'x' is an average of the PCs 0–5 days prior to an individual outbreak event, and the star represents the average position of the NPJ 5 days prior to all outbreak events. (b, d, & f) Composite trajectories showing the average evolution of the NPJ within the NPJ Phase Diagram during the 5-day period prior to an event.

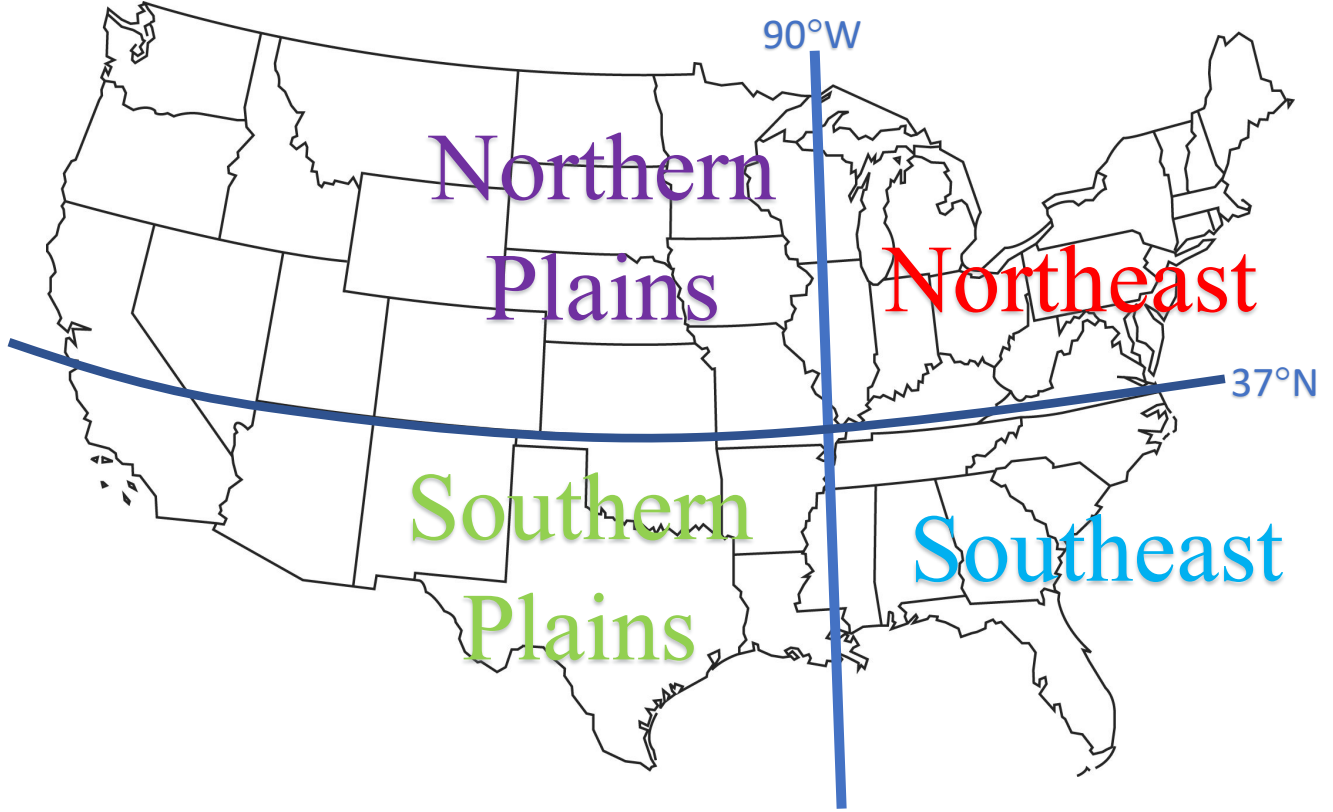
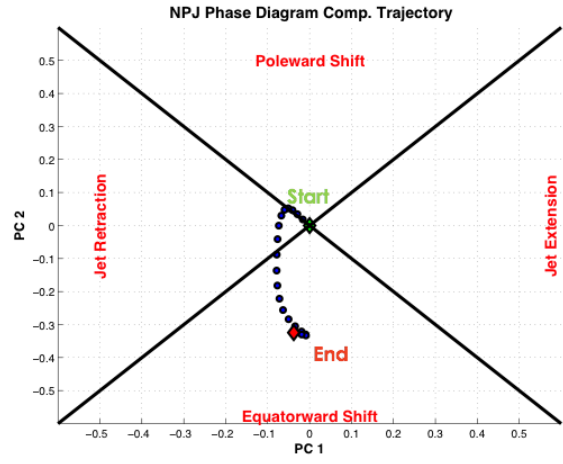
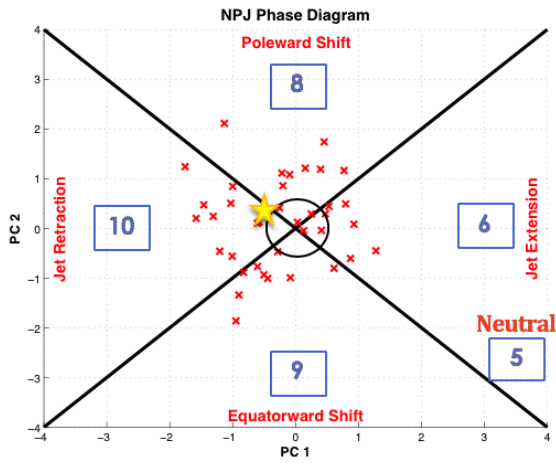


Fig 8: Schematic illustrating the classification scheme for the four geographic regions discussed in the text.

a & b: Northern Plains outbreaks (N=38)



c & d: Southern Plains outbreaks (N=70)

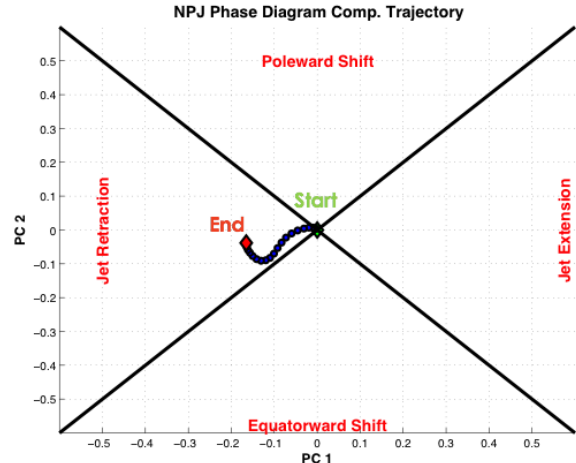
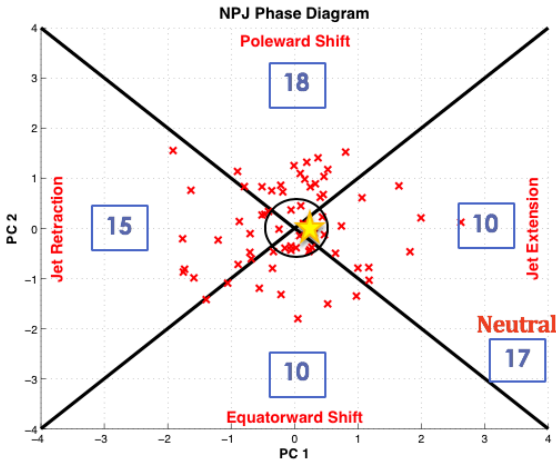
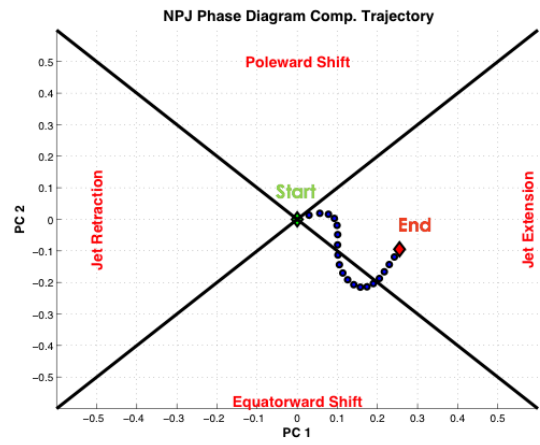
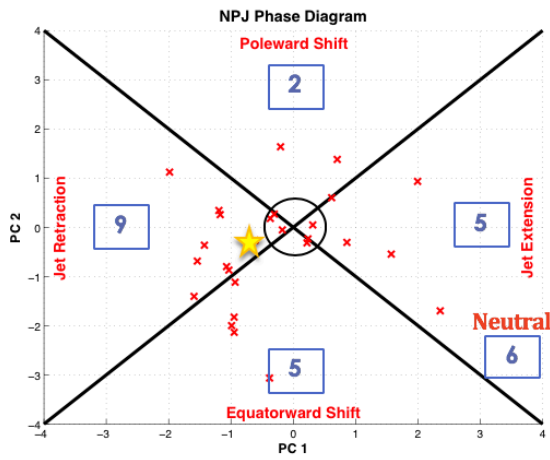


FIG 9. (a, c, e, & g) NPJ Phase Diagrams where each 'x' is an average of the PCs 0–5 days prior to an individual outbreak event, and the star represents the average position of the NPJ 5 days prior to all outbreak events. (b, d, f & h) Composite trajectories showing the average evolution of the NPJ within the NPJ Phase Diagram during the 5-day period prior to an event.

e & f: Northeast outbreaks (N=27)



g & h: Southeast outbreaks (N=54)

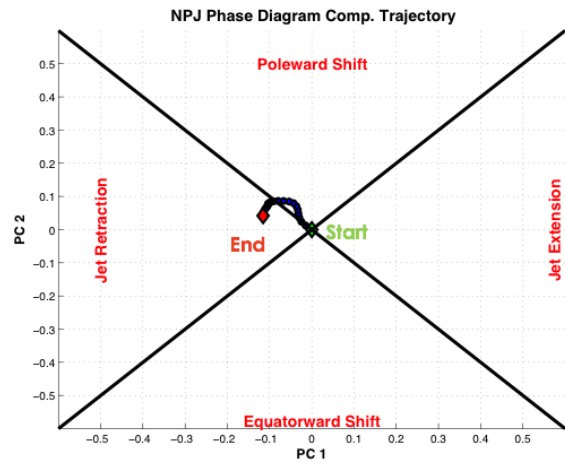
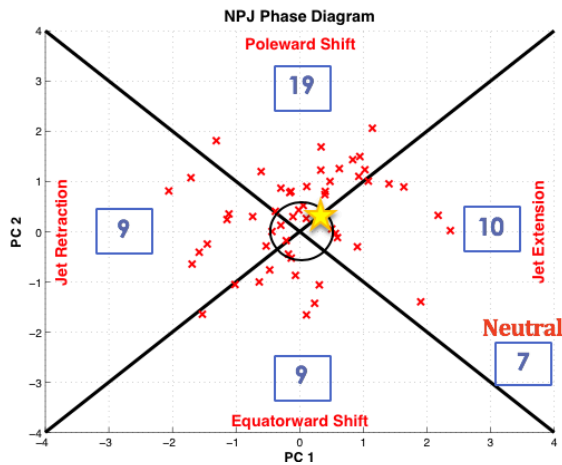


FIG 9. (continued) (a, c, e, & g) NPJ Phase Diagrams where each 'x' is an average of the PCs 0–5 days prior to an individual outbreak event, and the star represents the average position of the NPJ 5 days prior to all outbreak events. (b, d, f & h) Composite trajectories showing the average evolution of the NPJ within the NPJ Phase Diagram during the 5-day period prior to an event.

a & b: Top 20 most destructive outbreaks

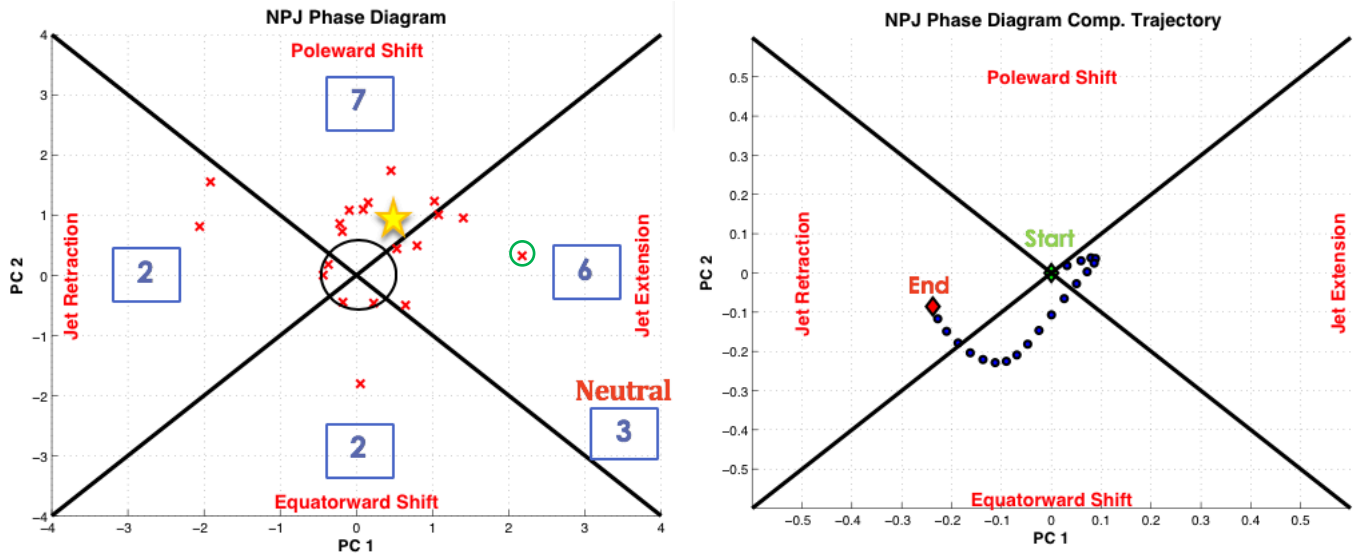


FIG 10. (a) NPJ Phase Diagrams where each ‘x’ is an average of the PCs 0–5 days prior to an individual outbreak event, and the star represents the average position of the NPJ 5 days prior to all outbreak events. Veteran’s Day 2002 Outbreak circled in green (b) Composite trajectories showing the average evolution of the NPJ within the NPJ Phase Diagram during the 5-day period prior to an event.

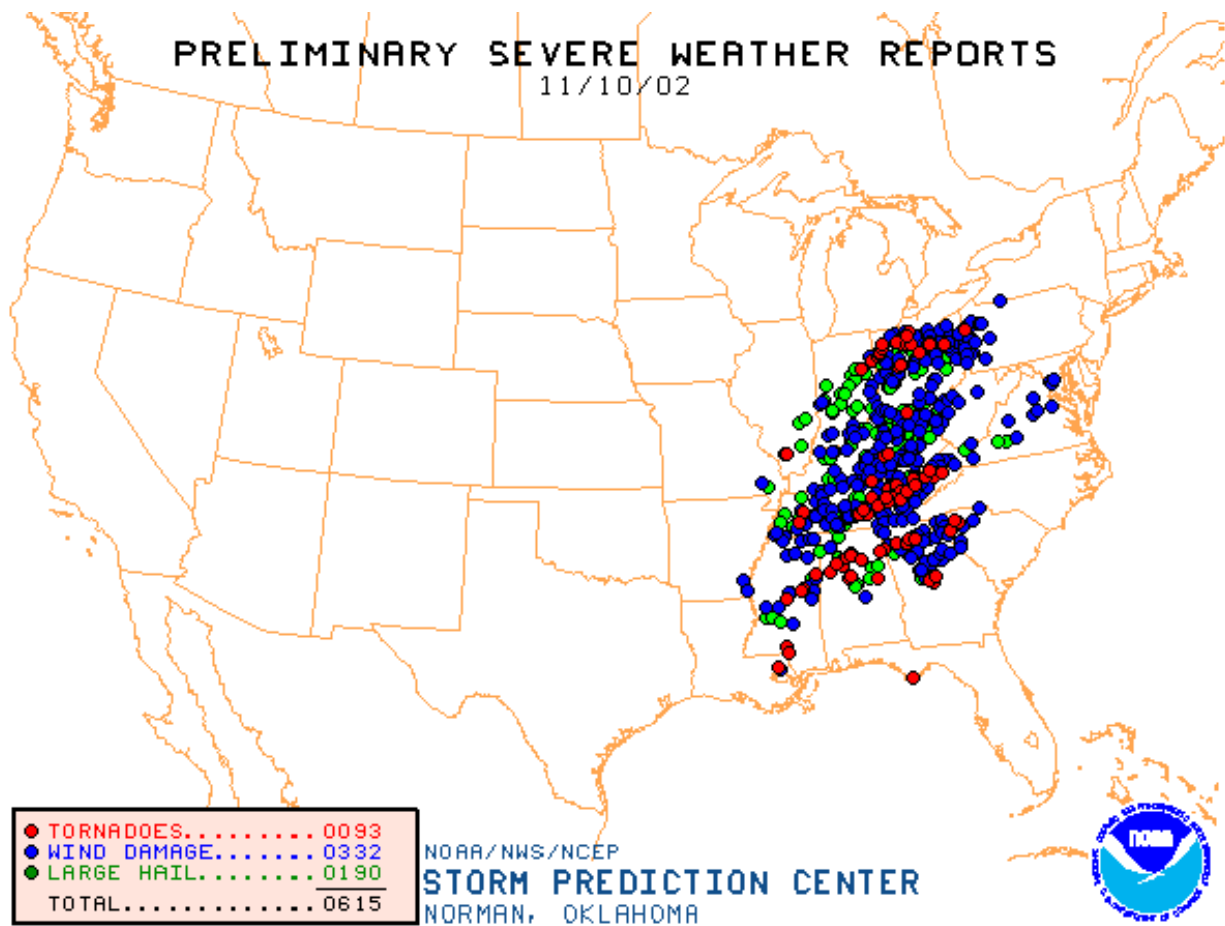
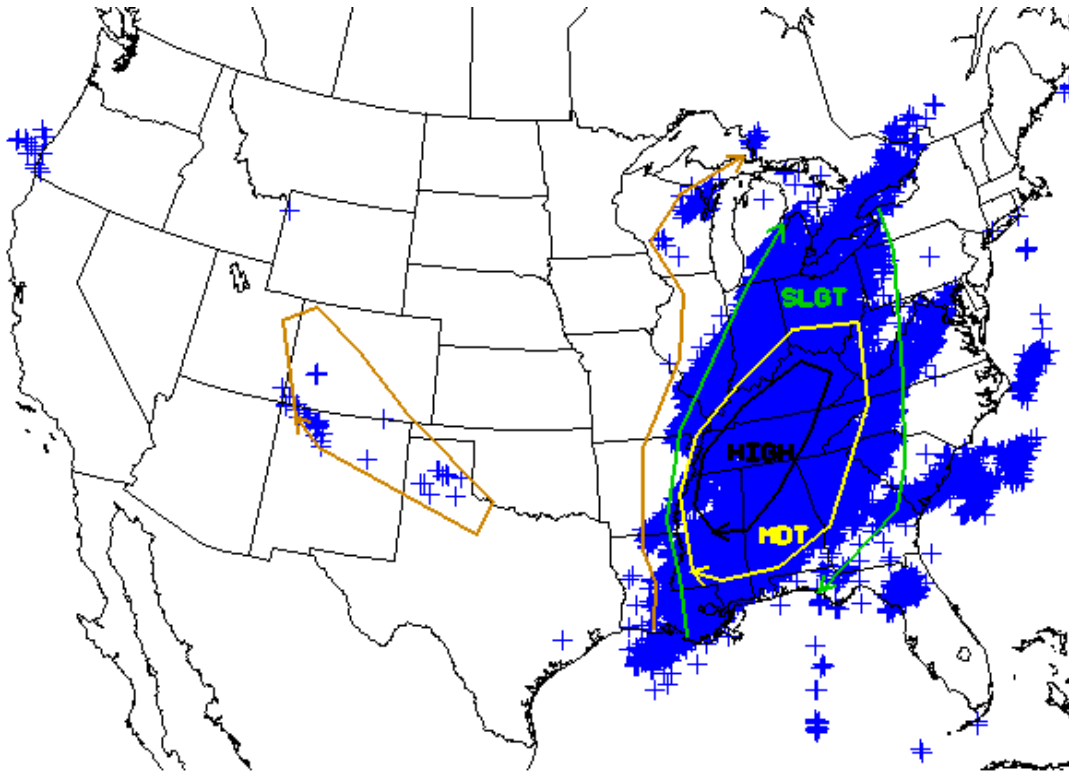


FIG 11. Storm Prediction Center's storm reports for 1200 UTC 10 November 2002 – 1200 UTC 11 November 2002.



20021110 06Z DAY1 and 20021110/12Z to 20021111/12Z LIGHTNING  
(217291 total strikes)

FIG 12. Storm Prediction Center's Day 1 Convective Outlook issued at 0600 UTC 10 November 2002 for 1200 UTC 10 November 2002 – 1200 UTC 11 November 2002.

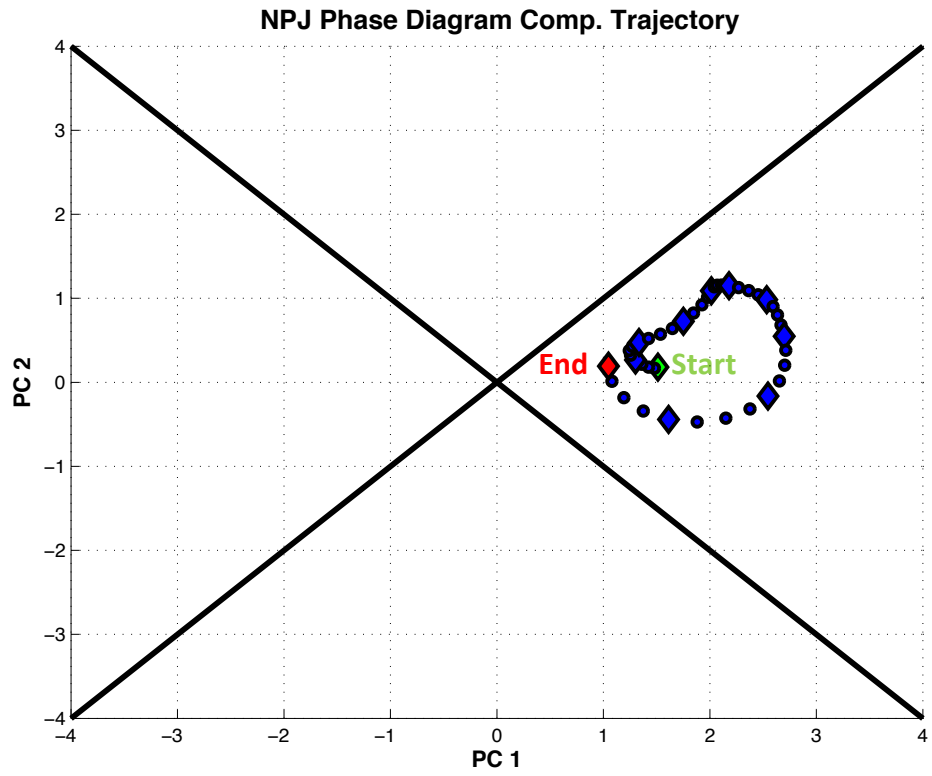
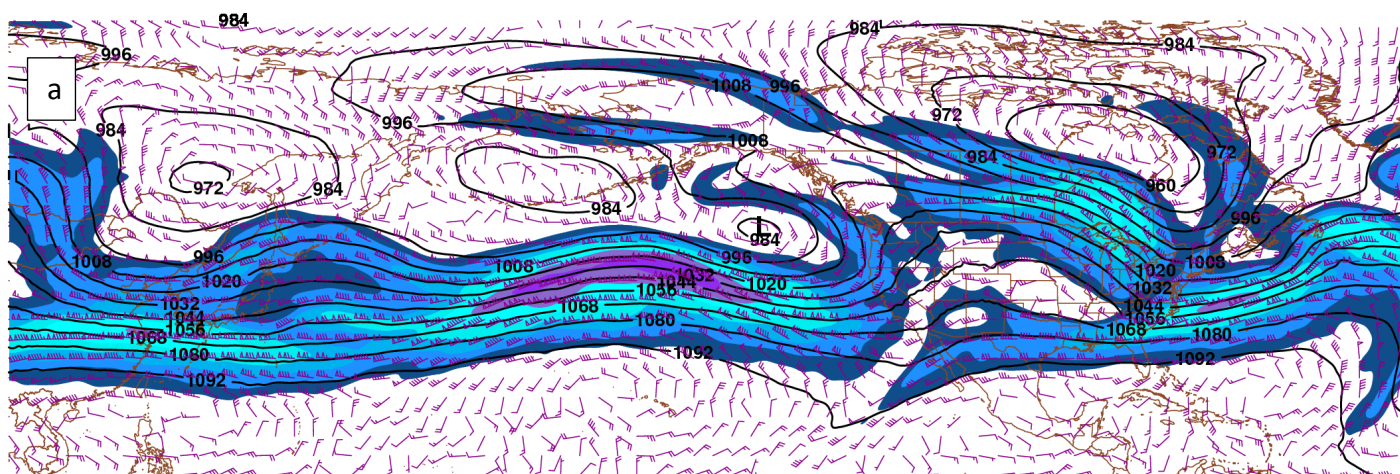
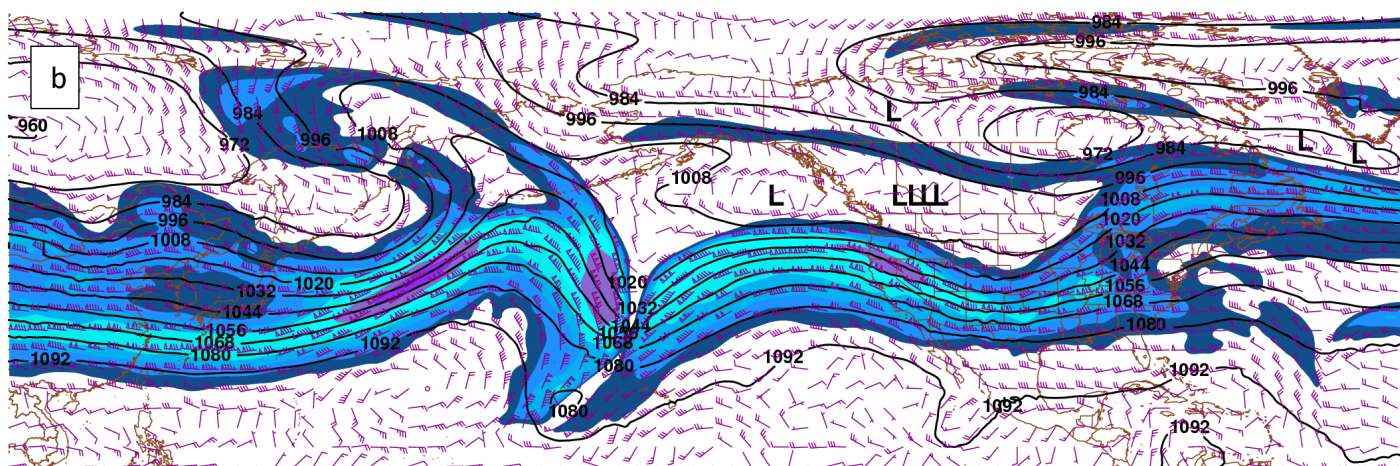


FIG 13: Trajectory of the NPJ within the NPJ Phase Diagram during the 10-day period prior to the Veterans Day Outbreak (10 November 2002).



021107/1200F000 250 hPa height and wind



021110/1200F000 250 hPa height and wind



FIG 14. a) 250-hPa winds (kts) plotted in barbs and the fill pattern, and geopotential heights (dam) at 1200 UTC 07 November 2002. b) As in (a), but for 1200 UTC 10 November 2002.

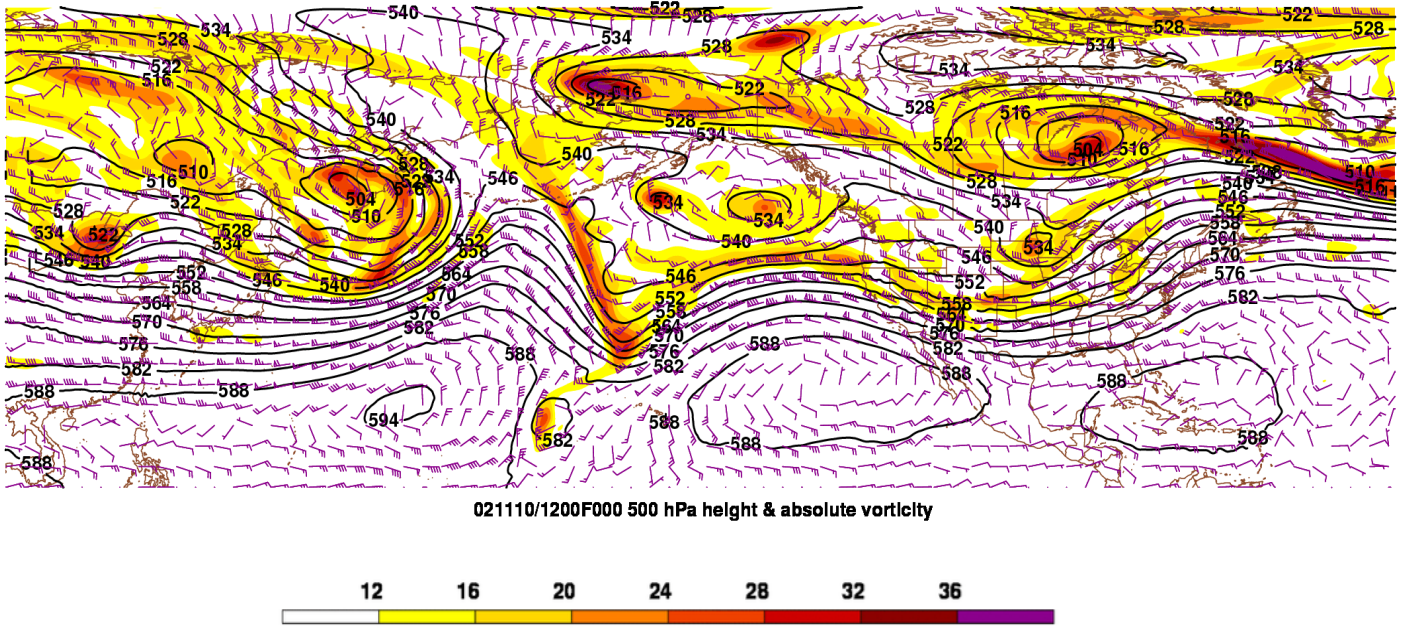
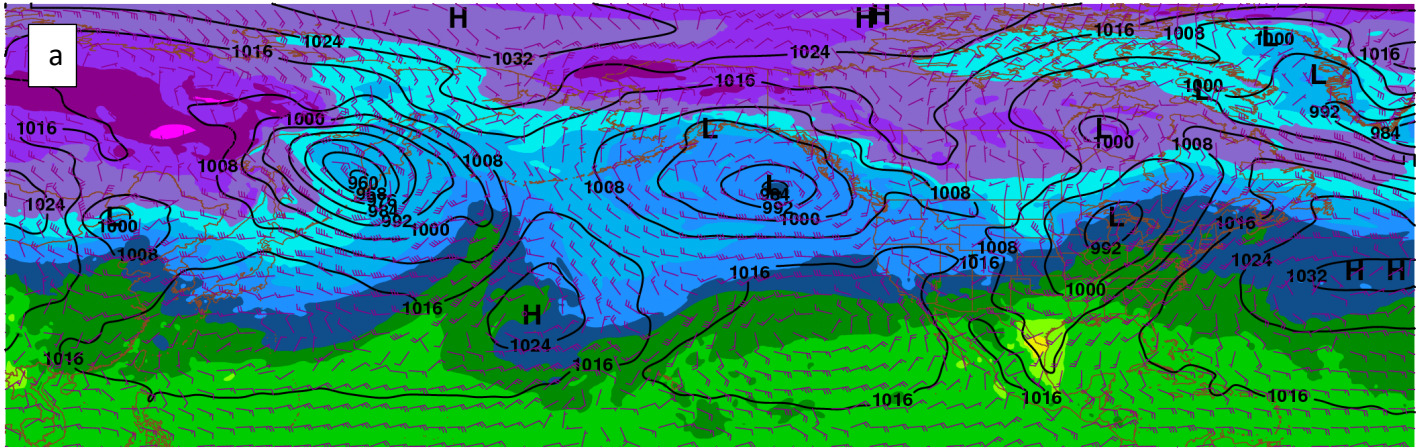
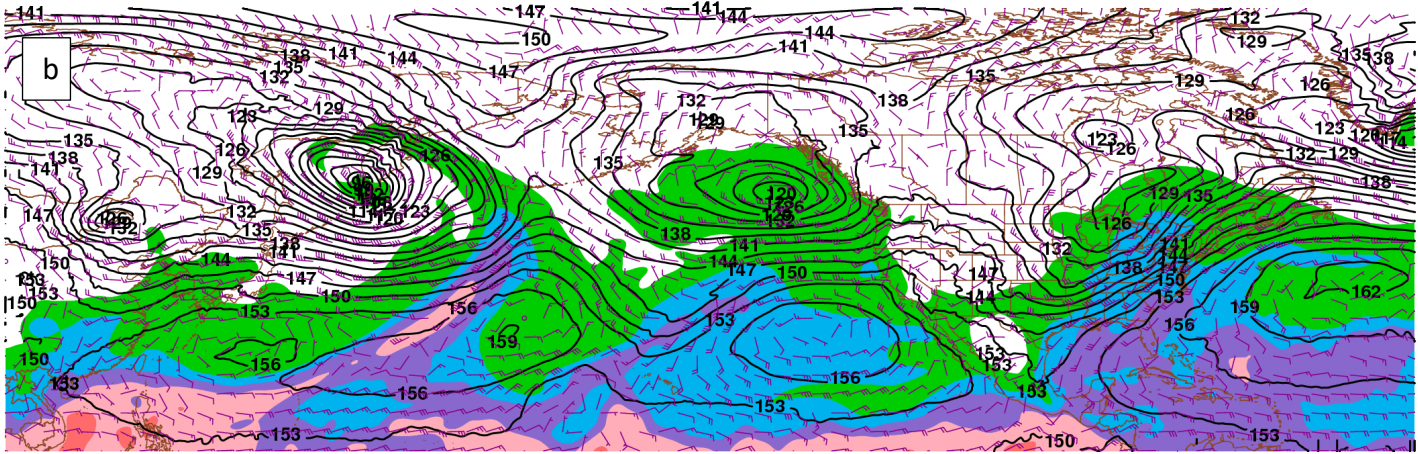
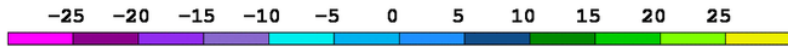


FIG 15. 500-hPa winds (kts) plotted in barbs, vorticity plotted in the fill pattern and scaled by  $10^5$  ( $s^{-1}$ ), and geopotential heights (dam) contoured at 1200 UTC 10 November 2002.



021110/1200F000 850 hPa temp and mslp



021110/1200F000 850 hPa precipitable water and height



FIG 16. a) 850-hPa temperature ( $^{\circ}\text{C}$ ) plotted in fill pattern, wind (kts) plotted in barbs, and mean sea-level pressure contoured (hPa) at 1200 UTC 10 November 2002. b) Precipitable water (mm) plotted in the fill pattern, 850-hPa wind (kts) plotted in barbs, and mean sea-level pressure contoured (hPa) at 1200 UTC 10 November 2002.

72327 BNA Nashville

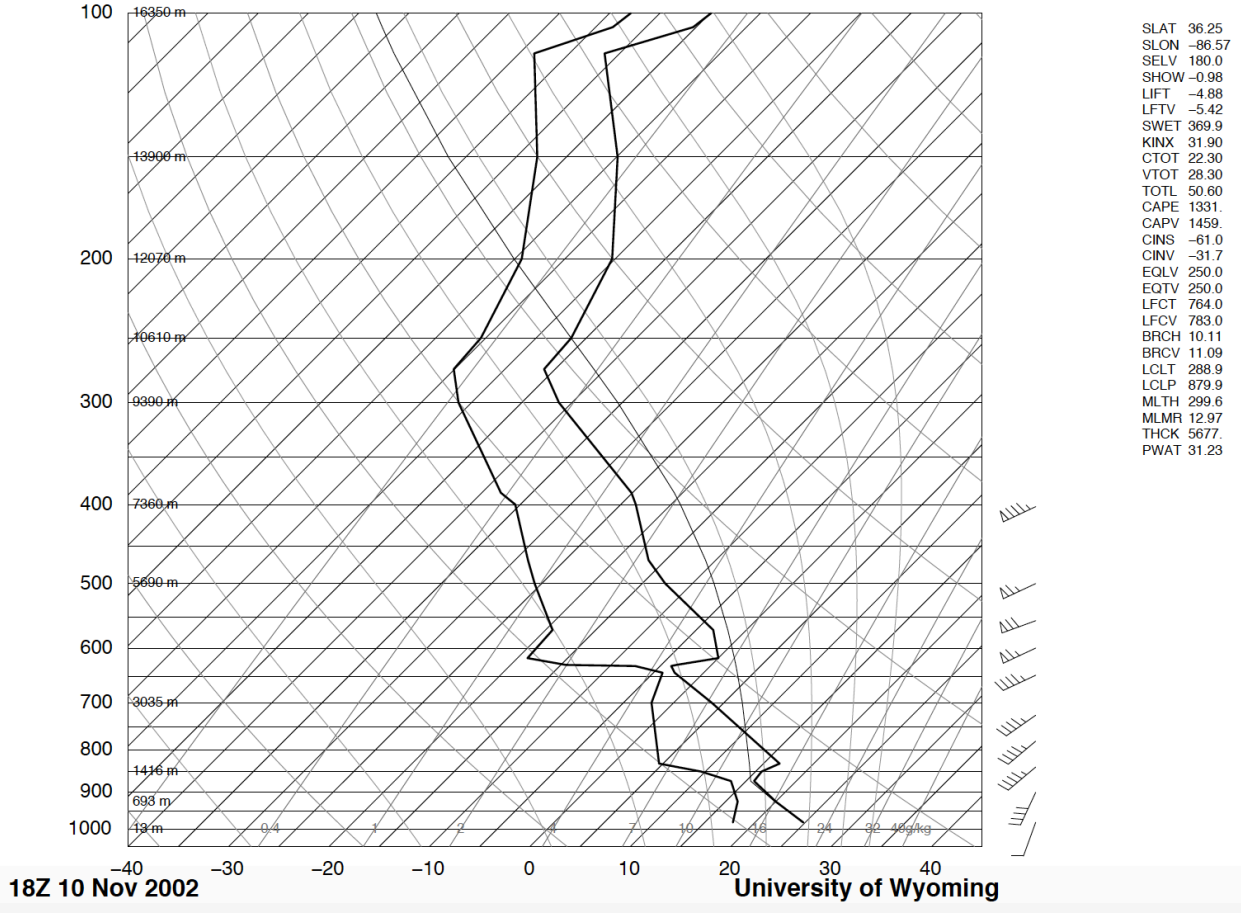


FIG 17. Sounding launched from Nashville, TN (BNA) at 1800 UTC 10 November 2002 (Sounding courtesy of the University of Wyoming)

CFSR 950 hPa potential temperature (K), winds (kts), and frontogenesis ( $^{\circ}\text{C}$ ) / 3 hour / 100 km  
Valid at: 2002-11-11-0000 UTC

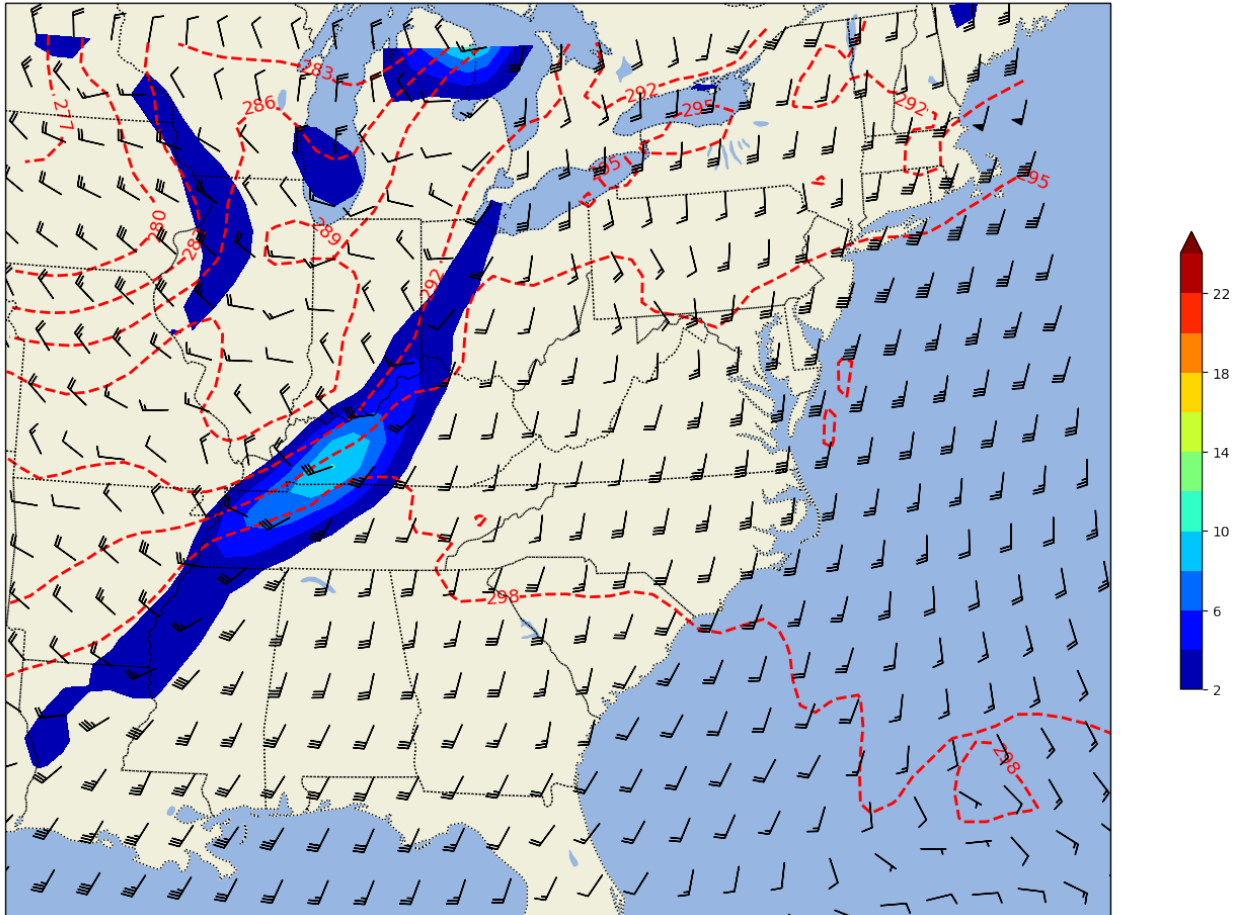


FIG 18. 950-hPa Frontogenesis ( $^{\circ}\text{C}$  / 3hr/100km) plotted in the fill pattern, winds (kts) in barbs, and potential temperature (K) contoured at 0000 UTC 11 November 2002.